Adsorption 11: 35–50, 2005

Cooperative and Competitive Adsorption of Ethylene, Ethane, Nitrogen and Argon on Graphitized Carbon Black and in Slit Pores

D.D. DO* AND H.D. DO
Department of Chemical Engineering, University of Queensland, St. Lucia, Qld 4072, Australia
duongd@cheque.uq.edu.au

Received May 19, 2004; Revised October 20, 2004; Accepted November 3, 2004

Abstract. In this paper we investigate the mixture adsorption of ethylene, ethane, nitrogen and argon on graphitized thermal carbon black and in slit pores by means of the Grand Canonical Monte Carlo simulations. Pure component adsorption isotherms on graphitized thermal carbon black are first characterized with the GCMC method, and then mixture simulations are carried out over a wide range of pore width, temperature, pressure and composition to investigate the cooperative and competitive adsorption of all species in the mixture. Results of mixture simulations are compared with the experimental data of ethylene and ethane (Friederich and Mullins, 1972) on Sterling FTG-D5 (homogeneous carbon black having a BET surface area of 13 m^2/g) at 298 K and a pressure range of 1.3–93 kPa. Because of the co-operative effect, the Henry constant determined by the traditional chromatography method is always greater than that obtained from the volumetric method.

1. Introduction

Adsorption behavior on open surfaces or in pores has been studied extensively in the literature by various approaches, ranging from empirical approaches to those that have basis in classical thermodynamics (Yang, 1987; Jaroniec and Madey, 1988). One of the earliest theoretical studies on mixture adsorption is the Ideal Adsorption Solution Theory (IAST) of Myers and Prausnitz (1965). This approach as well as many later theoretical studies have been used by many researchers for studying adsorption equilibria of mixtures (for example, LeVan and Vermeulen, 1981; Moon and Tien, 1987; Russel and LeVan, 1996, 1997; Taqvi and LeVan, 1997; Staudt et al., 1998; Keller et al., 1999). Tabulation of adsorption mixture data, mostly on porous activated carbon and other porous materials, are also available (Reich et al., 1980; Costa et al., 1981, 1989; Kaul, 1984; Valenzuela and Myers, 1989). Recently more advanced tools of Monte Carlo simulation (Steele, 1999, 2002), molecular dynamics simulation (MD) and density functional theory (Latoskie et al., 1993a, 1993b, 1997; Olivier, 1995) have been applied to solve this problem, and these tools use more fundamental parameters than those used in classical theories. Usually these parameters are the molecular parameters associated with the interaction between interaction sites of the molecules. In particular, the MC and MD methods are suitable to study simple molecules as well as complex ones that possess orientation and discrete charges. The greater application of these tools in recent years is mostly due to their power in describing adsorption behavior from a single information of a potential energy model between fluid particles and a model for solid-fluid interaction.

In this paper we studied mixtures of symmetrical linear molecules and spherical molecules by using the Grand Canonical Monte Carlo simulation. Here we chose ethylene, ethane, nitrogen and argon as model adsorbates, and studied their adsorption in slit pores as

*To whom correspondence should be addressed.

well as on graphitized thermal carbon black. The latter has been used as a reference material for characterizing carbon surface (Kruk et al., 1999; Gardner et al., 2001). Pure component adsorption of ethane and ethylene on graphitized thermal carbon black has been recently studied (Do and Do, 2004), and the objective of this paper is then to investigate the co-operation and competition of the mixtures of ethane and ethylene as well as mixtures with nitrogen and argon on open surface of graphitized thermal carbon black and in slit pores of various sizes. Isosteric heat from adsorption of mixture is also obtained from the GCMC through the fluctuation theory. For the case of ethane and ethylene mixture, limited data on adsorption isotherms were available from the work of Friedrich and Mullins (1972) for Sterling FTG-D5 (a homogeneous carbon black with a BET surface area of 13 m^2/g) and they are used to confirm the validity of the model.

1.1. Two-Center Potential Model

One direct approach in dealing with linear molecules is to treat every atom on these molecules as one site in the calculation of intermolecular interaction (Chen and Siepmann, 1999). This approach is time-consuming and often it does not add extra insight into adsorption from the alternative approach of united atom. In the latter approach a number of atoms are grouped together to constitute one interaction site. For the case of ethylene for example, there are two such united atoms, each one of which contains one carbon atom and two hydrogen atoms. In this paper, we consider a United Atom (UA) model for ethane and ethylene, whose molecular parameters are given in Martin and Siepmann (1998) and Wick et al. (2000), respectively. The site-site interaction is described by the classical 12-6 Lennard-Jones potential equation. To be explicit, the interaction potential energy of a site a on a molecule i and a site b on a molecule j is given by:

$$\varphi_{i,j}^{(a,b)} = 4\varepsilon^{(a,b)}\left[\left(\frac{\sigma^{(a,b)}}{r_{i,j}^{(a,b)}}\right)^{12} - \left(\frac{\sigma^{(a,b)}}{r_{i,j}^{(a,b)}}\right)^{6}\right] \quad (1a)$$

where the subscript denotes for molecule while the superscript indicates the interaction site. Each interaction site is characterized by two parameters. For example, for site "a" these parameters are the collision diameter ($\sigma^{(a,a)}$) and the well depth of the interaction energy ($\varepsilon^{(a,a)}$). Since the two groups of ethylene and ethane are identical, the ethylene or ethane molecule is characterized by one value of the collision diameter, one value of the well depth of the interaction energy and the distance between the two interaction sites. Given the site-site interaction energy, the molecule-molecule interaction energy is then calculated from:

$$\varphi_{i,j} = \sum_{a=1}^{M}\sum_{b=1}^{M}\varphi_{i,j}^{(a,b)} \quad (1b)$$

where M is the number of sites on a molecule (in this case $M = 2$). The values of these parameters for ethylene and ethane are given in Table 1.

Table 1. Parameters for ethane and ethylene for the UA-TraPPE potential model.

	UA model		
Species	σ (A)	ε/k (K)	ι (A)
Ethane	3.75	98	1.54*
Ethylene	3.675	85	1.33**

*Carbon-carbon σ bond length; **carbon-carbon double bond length.

For nitrogen, it is modeled as two dispersive sites (located at nitrogen atom centers) and a set of discrete charges to account for the quadrupole and higher moments (the quadrupole moment of nitrogen is -4.9×10^{-40} Cm^{-2}). This quadrupole can be described by specifying a set of discrete charges and their locations on each nitrogen molecule. Having this information, the electrostatic interaction between a charge "α" on a molecule "i" and a charge "β" on a molecule "j" is determined via the Coulomb law of electrostatic interaction (Tipler, 1999):

$$\varphi_{q;i,j}^{(\alpha,\beta)} = \frac{1}{4\pi\varepsilon_0}\cdot\frac{q_i^{\alpha}q_j^{\beta}}{r_{i,j}^{(\alpha,\beta)}} \quad (2a)$$

where ε_0 is the permittivity of free space ($\varepsilon_0 = 10^7/(4\pi c^2) = 8.8543 \times 10^{-12}$ $C^2J^{-1}m^{-1}$; c is the speed of light), $r_{i,j}^{(\alpha,\beta)}$ is the distance between two charges α and β on the molecules i and j, respectively, q_i^{α} is the value of the charge α on the molecule i and q_j^{β} is the value of the charge β on the molecule j. The total electrostatic interaction between two molecules takes the form:

$$\varphi_{q;i,j} = \sum_{\alpha=1}^{M_q}\sum_{\beta=1}^{M_q}\varphi_{q;i,j}^{(\alpha,\beta)} \quad (2b)$$

Here M_q is the number of charges on the molecule. It may not be the same as the number of LJ sites, M, and their positions may also not be the same as those for dispersion sites.

The potential model that we use in this paper for nitrogen is the one proposed by Murthy et al. (1983). Each nitrogen molecule has 2 LJ sites and 3 discrete charges ($M = 2$ and $M_q = 3$). One positive charge (0.810e) is at the center of the molecular axis joining the two centers of nitrogen atoms and the two symmetric negative charge (−0.405e) are on the same axis with a distance of 1.1 A from each other. The collision diameter and the well-depth of the interaction energy of a nitrogen atom are:

$$\sigma^{N-N} = 3.32\,\text{A}, \quad \varepsilon^{N-N}/k = 36.4\,\text{K}$$

The distance between the two LJ sites is the same as that between two negative charges (i.e. the charge is on the LJ site).

Argon is treated as a spherical molecule, and the molecular parameters for argon are $\sigma = 3.405$ A, $\varepsilon/k = 119.8$ K.

2. Theory

The simulation tool used in this paper is the Grand Canonical Monte Carlo (GCMC) simulation (Norman and Filinov, 1969; Adams, 1975). This tool is described in details in Allen and Tildesley (1987). In the Grand Canonical Monte Carlo (GCMC) simulation, we specify temperature, volume (pore volume) and the chemical potential. This simulation is suitable for studying adsorption in pores as well as on solid surfaces. The common feature shared by all Monte Carlo simulation methods is that a Markov chain of molecular configurations is produced. Any properties of interest can be obtained by averaging over this chain. In GCMC, there are three different moves used to generate the Markov chain, which is composed of a series of molecular configurations. The first move is the displacement. For linear molecules, we have an additional move, which is the changing of particle's orientation. The two remaining moves in the GCMC are the insertion and removal of a particle. In the insertion move, a particle is inserted at a random position within the simulation box, while in the removal move a particle is selected in random and removed from the box. For the case of linear particle in insertion move, we randomly select a position for the center of mass and choose a random orientation on a sphere for the molecular axis. These two moves are either accepted or rejected when appropriate probabilities of acceptance are either greater or lower than a random number generated uniformly between 0 and 1. The additional move which is very useful for mixtures is the identity swap, which was introduced by Cracknell et al. (1993).

2.1. *Solid-Fluid Interaction Energy*

In the GCMC simulation of adsorption, the external force exerted by the presence of solid surfaces can be evaluated once a model for surface or pore is chosen. In this paper, we take a simple model of surface and slit pore, where the surface is assumed to be flat and homogeneous (structureless). It is infinite in the two lateral directions x and y. Because of the infinite nature of the pore, we will work with a finite simulation cell with periodic boundary conditions in the x and y directions. The interaction potential energy between a particle and the homogeneous solid carbon substrate is calculated by the well-known 10-4-3 Steele potential (Steele, 1973, 1974). The interaction between a site a on a molecule j and the surface takes the following form:

$$\varphi_{i,s}^{(a)} = 4\pi\rho_C\,\varepsilon^{(a,s)}[\sigma^{(a,s)}]^2\Delta\left\{\frac{1}{5}\left(\frac{\sigma^{(a,s)}}{z_i^{(a)}}\right)^{10} - \frac{1}{2}\left(\frac{\sigma^{(a,s)}}{z_i^{(a)}}\right)^{4} - \frac{[\sigma^{(a,s)}]^4}{6\Delta\left(0.61\Delta + z_i^{(a)}\right)^3}\right\} \tag{3a}$$

where ρ_C is the volumetric carbon atom density (114 nm^{-3}), Δ is the spacing between two adjacent graphene layers (3.35 A), and $z_i^{(a)}$ is the shortest distance between the site a on the molecule i and the plane passing through all carbon atoms of the outermost layer of carbon wall. The solid-site molecular parameters, the collision diameter and the interaction energy, are calculated from the Lorentz-Berthelot mixing rule.

$$\sigma^{(a,s)} = \left(\sigma^{(a,a)} + \sigma^{(s,s)}\right)/2 \tag{3b}$$

$$\varepsilon^{(a,s)} = (1 - k_{sf})\sqrt{\varepsilon^{(a,a)}\varepsilon^{(s,s)}} \tag{3c}$$

The molecular parameters of carbon atom are $\sigma^{(s,s)} = 3.4$ A and $\varepsilon^{(s,s)}/k_B = 28$ K. The well depth of the solid-fluid interaction energy (Eq. 3(c)) is adjusted with the introduction of the solid-fluid binary interaction parameter, k_s such that the experimental Henry

constant is reproduced by the GCMC simulations. Fitting of the pure component Henry constant of ethylene and ethane on graphitized thermal carbon black (Avgul and Kiselev, 1970), we have found that the binary interaction parameter is −0.05, −0.02, −0.04 and 0.02 for ethylene, ethane, nitrogen and argon respectively. Knowing the site-surface interaction energy as given in Eq. (3a), the molecule-surface interaction energy is calculated from:

$$\varphi_{i,s} = \sum_{a=1}^{M} \varphi_{i,s}^{(a)} \tag{3d}$$

In the GCMC simulations of adsorption on graphitized thermal carbon black and in slit pores we use the following parameters. Generally, the box length is chosen to be equal to 10 times the collision diameter, and the cut-off radius is taken to be half of the box length. The number of cycle in the equilibration step and in the collecting statistics step is 50,000 each, and in each cycle we have N displacements and rotations (N is the number of particles). For the typical Monte Carlo parameters listed above, the computation time is of the order of ten hours to complete an isotherm for the case of linear molecules. The deviation of the simulation results is of the order of the size of the symbols used in the plots.

For simulations of an open graphitized thermal carbon black surface, we use a slit pore having width of 80 A. This width is large enough for that slit pore to mimic two independent surfaces. In presenting the GCMC simulation results we plot them as (i) average surface excess (for open surface) and average pore density (for slit pore) versus pressure, (ii) 2D-plot of local density versus the distance across the pore, and (iii) 3D-plot of local density versus the distance across the pore and the angle θ formed between the molecular axis and the z-direction (perpendicular to the pore surface). The average surface excess and the average pore density are defined as

$$\Gamma_{av} = \frac{\langle N \rangle}{L_x L_y} - \frac{\rho \lfloor L_x L_y (H - \sigma_{ss}) \rfloor}{L_x L_y} \tag{4a}$$

$$\rho_{av} = \frac{\langle N \rangle}{L_x L_y (H - \sigma_{ss})} \tag{4b}$$

where ρ is the bulk molecular density, L_x and L_y are the box lengths in the x and y-directions, respectively, and $\langle N \rangle$ is the ensemble average of the number of particle in the pore. Here the pore width H is defined as the distance between the plane passing through all carbon atom centers of the outermost layer of one wall and the corresponding plane of the opposite wall. In this paper, we define the accessible pore width as $H - \sigma_{ss}$.

To study how molecules are layered and their distribution from the surface, we study the local density as a function of distance from a pore surface. It is defined as:

$$\rho(z) = \frac{\langle \Delta N(z) \rangle}{L_x L_y \Delta z} \tag{5}$$

where $\Delta N(z)$ is the number of ethylene molecules whose centers of mass are located in the segment having boundaries at z and $z + \Delta z$, and L_x and L_y are the box lengths in the x and y-directions, respectively. This plot of $\rho(z)$ versus z does not tell us about the way how molecules are oriented. To do this, we need to study the 3D-plot of local density distribution, and this local density distribution is calculated from:

$$\rho(z, \theta) = \frac{\langle \Delta N(z, \theta) \rangle}{L_x L_y \Delta z \sin\theta \Delta\theta} \tag{6}$$

where $\Delta N(z, \theta)$ is the number of ethylene molecules whose centers of mass are located in the segment having boundaries $z, z + \Delta$, and the angle between the molecular axis and the z direction falls between θ and $\theta + \Delta\theta$. This plot of $\rho(z, \theta)$ versus z and θ allows us to evaluate the preferential orientation of the molecules located at various distances from the wall surface. An angle of 0 means that the molecule lies perpendicular to the pore wall, while a value of $\pi/2$ means that the molecule is parallel to the pore surface. All our subsequent plots are presented as LJ-non-dimensional density, defined as $\rho^* = \rho\sigma^3$.

The utility of the GCMC simulations is not only in the generation of adsorption isotherm and the microscopic configuration of molecules, but also in the calculation of various thermodynamics quantities, for example the isosteric heat. Using the fluctuation theory, the isosteric heat is calculated from Nicholson and Parsonage (1982):

$$q_{\text{iso}} \frac{\langle U \rangle \langle N \rangle - \langle UN \rangle}{\langle N^2 \rangle - \langle N \rangle \langle N \rangle} + k_B T \tag{7}$$

where N is the number of particle and U is the configuration energy of the system.

3. Results and Discussions

We study the mixture adsorption of the following mixtures: (1) ethylene/Ar, (2) ethylene/nitrogen, and (3) ethylene/ethane. The temperatures chosen in this simulation study is 200 K. At this temperature, the first two systems have one component as sub-critical fluid and the other as super-critical fluid, while in the last system (ethylene/ethane) both components are sub-critical fluids.

3.1. Ethylene-Argon Mixture

First we study the mixture of ethylene and argon. Often carried out in the literature to determine the Henry constant of a solute is the application of the gas-solid chromatography. A carrier gas, usually argon or nitrogen, is used to carry a minute amount of adsorbate (solute) into a column packed with solid adsorbent. Due to adsorption this adsorbate spends longer time than the fluid residence time, and it elutes from the column at the so-called retention time. After appropriately isolating the dead volume, the corrected retention time is calculated and hence the Henry constant is derived. This Henry constant is then taken as a measure of affinity of the adsorbate towards the solid adsorbent. We will show in this section that such a conclusion is not strictly correct as the carrier gas does affect the adsorption of adsorbate.

First we consider adsorption of mixture of ethylene and argon in slit pores of 10 and 15 A, typically of pore sizes found in activated carbon. The temperature studied is 200 K, at which ethylene is a sub-critical fluid while argon is a super-critical fluid (the critical temperatures of ethylene and argon are 282.4 and 150.8 K, respectively).

10 A Pore Width

It has been implicitly assumed in the literature that by using an inert gas as a carrier the adsorption of solute in mixture is the same as the adsorption of pure adsorbate in a volumetric apparatus. We show in Fig. 1 the GCMC results for the case of ethylene at 200 K and a pore width of 10 A, with Fig. 1(a) showing the results at low pressure range (0–500 Pa) while Fig. 1(b) for higher pressure range (up to 10,000 Pa).

In this figure we plot the average pore density (Eq. 4(b)) versus the partial pressure of ethylene. The curve with triangle symbol is the result for the case of pure ethylene, while the curve with circle symbol is for the case of ethylene-argon mixture. The partial pressure of argon in the case of mixture is maintained constant at 1×10^5 Pa to mimic the chromatography conditions. We observe that at low pressures the adsorption of ethylene in the presence of argon is greater than that in the case of pure ethylene. At first, it is thought that in the presence of another adsorbate (argon) there will be a competition between them and as a result the adsorbed amount of ethylene in the case of mixture should be less than that for the case of pure ethylene. The observed opposite behavior at low pressure seen in Fig. 1(a) is simply due to the fact that in that pressure range the surface is only fractionally covered and therefore there is no issue of competition for the available space on the

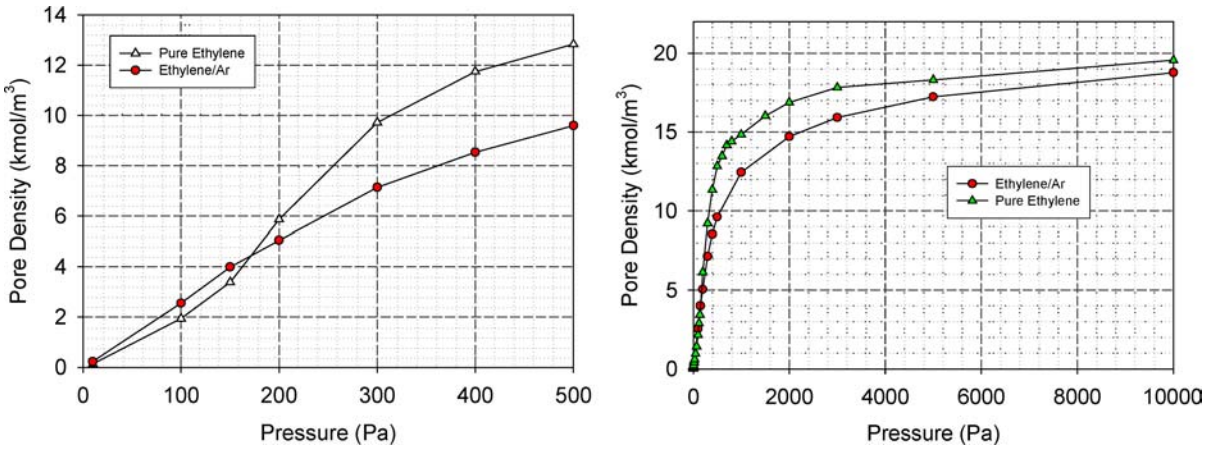

Figure 1. Adsorption isotherm of ethylene in slit pore of 10 A pore width (circle: mixture; triangle: pure component).

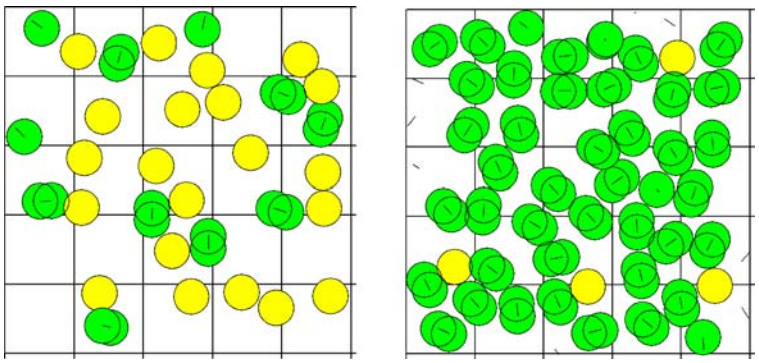

Figure 2. Snap shot of adsorption for the case of ethylene/argon mixture (a) ethylene partial pressure = 100 Pa; (b) ethylene partial pressure = 10,000 Pa.

surface for adsorption. The enhancement in the ethylene adsorption is due to the lateral interaction between ethylene and argon, increasing the amount of ethylene adsorbed compared to that in the case of pure ethylene. It must be borne in mind that argon does adsorb on the surface and its partial pressure is 100,000 Pa. Such an enhancement in adsorption is called the *cooperative* adsorption, and such co-operation is possible for practically all mixtures as long as the surface is only fractionally covered. However, when the partial pressure of ethylene is increased (greater than 200 Pa), the surface is fully covered with adsorbed molecules, ethylene and argon, and the *competition* for adsorption space will occur and as a result ethylene is dominantly favored by the surface because of its greater affinity with the solid surface. Eventually when the partial pressure is high enough the ethylene adsorbed concentration in the case of mixture will approach that in the case of pure ethylene (Fig. 2(b)). The distributions of ethylene and argon in pore and the orientation of ethylene can be studied with the investigation of the local density distribution. We shall postpone this discussion of the local distribution to the next sub-section where we will study 15 A pore.

Figure 2 shows a snapshot of ethylene and argon in the case of mixture adsorption, with Fig. 2(a) for the ethylene partial pressure of 100 Pa (co-operative region) and Fig. 2(b) for a partial pressure of 10,000 Pa (competitive region). In the co-operative region (Fig. 2(a)) in which the surface is fractionally covered, the presence of adsorbed argon on the surface helps to increase the adsorption of ethylene, resulting from the adsorbate-adsorbate interaction between ethylene molecules and argon molecules (note the proximity of argon molecules for each ethylene molecule in this figure). The difference between the pure ethylene case and the case of mixture of ethylene and argon can be seen in the shape of the adsorption isotherm. In the case of pure ethylene, the curve is linear at very low pressures (when ethylene molecules are far apart and no fluid-fluid interaction occurs). However, when pressure is higher, more ethylene molecules are adsorbed on the surface (surface is sill below the complete coverage) and the fluid-fluid interaction among ethylene molecules now comes into play and gives rise to a shaper increase in the rate of adsorption with pressure, resulting in the sigmoidal shape of the isotherm (Fig. 1(a)). On the other hand, in the case of mixture (where argon partial pressure is maintained constant at 100,000 Pa), the surface is covered with some argon molecules and it is these argon molecules that interact with any ethylene molecule adsorbed on the surface, resulting in a greater Henry constant (compared to the pure ethylene case).

In the competitive region (partial pressure of ethylene of 10,000 Pa), the surface is loaded with ethylene and argon molecules, with ethylene being the dominant species because of its greater affinity towards the surface (Fig. 2(b)). It is this competition for adsorption sites that ethylene simply displaces the weaker component argon from the surface (compare the snap shot of Fig. 2(b) with that in 2(a)). Also we note in Fig. 1(b) that in the competitive region that the adsorption of ethylene is greater in the case of pure ethylene, which is what we would expect from the presence of a second component (in this case, argon).

Thus what we see thus far is the cooperative adsorption when the total number of molecules is less than that required to fill a monolayer coverage, and

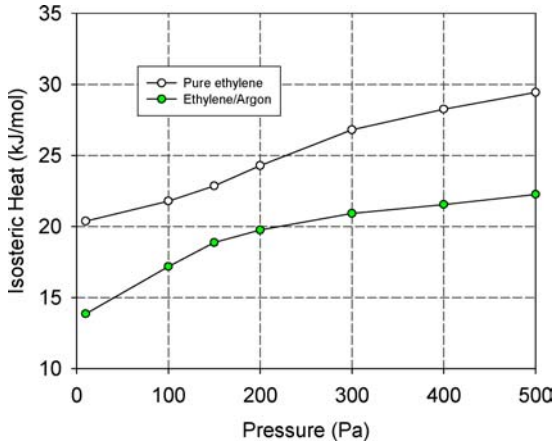

Figure 3. Heat of adsorption of pure ethylene and mixture of ethylene/argon versus the partial pressure of ethylene.

the competitive adsorption when the total number is greater than the monolayer amount.

Figure 3 shows the isosteric heat of adsorption for the case of pure ethylene and the case of mixture of ethylene and argon versus the partial pressure of ethylene (partial pressure of argon is maintained constant at 100,000 Pa). The lower heat in the latter case is due to the lower solid-fluid interaction of argon compared to that of ethylene. When the partial pressure of ethylene is greater, the adsorption is mostly contributed by ethylene. As a result, the isosteric heat of mixture is getting close to that of pure ethylene. For example, at 10,000 Pa of ethylene in mixture, the isosteric heat is 28.8 kJ/mol, compared to 33.2 kJ/mol for the case of pure ethylene.

15 A Pore Width

We have seen the co-operative and competitive adsorption in the case of 10 A pore. Let us now turn to a larger pore to investigate how significant is this phenomenon when the solid-fluid interaction is weaker in larger pores compared to that in smaller pores. We consider a 15 A pore. The results are shown in Figs. 4(a) and (b) for low pressure and higher pressure ranges, respectively. The phenomenon of cooperative and competitive is again observed for this 15 A pore, but the extent of the cooperative is much less than that in the case of 10 A. This is due to the stronger affinity with solid surface for the latter case, as shown in the lower pressure at which the cooperative mode is switched to the competition mode. In the case of 10 A pore, the switch-over pressure is about 170 Pa (Fig. 1(a)) while that in the case of 15 A is 2,200 Pa (Fig. 4(a)).

To investigate the adsorption layering and orientation, we need to study the local density distribution. Figure 5 shows the local density distribution as a function of distance from the pore surface for $P = 1{,}500$ Pa and 10,000 Pa. The first pressure is for co-operative region, and the latter is for competition region.

In the *co-operative* region of partial pressure of ethylene = 1,500 Pa and argon pressure of 100,000 Pa (Fig. 5(a)), both ethylene and argon molecules are adsorbed on the two contact layers close to the surface and the inner core is free of any adsorbed molecules (15 A pore can accommodate 3 layers). The contact layers are only fractionally covered, and the amounts adsorbed of these two species are comparable. The fluid-fluid interaction between argon and ethylene helps to enhance the

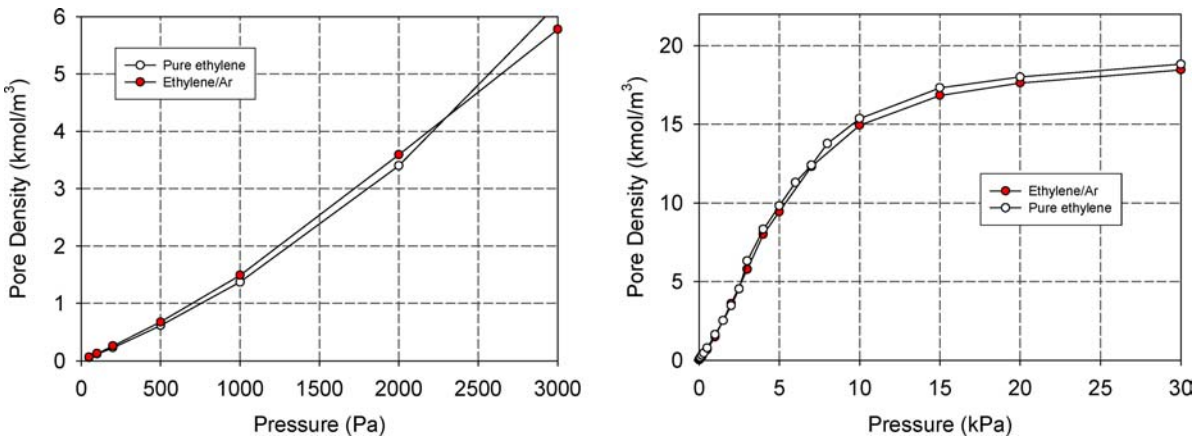

Figure 4. Adsorption isotherm of ethylene in slit pore of 15 A pore width.

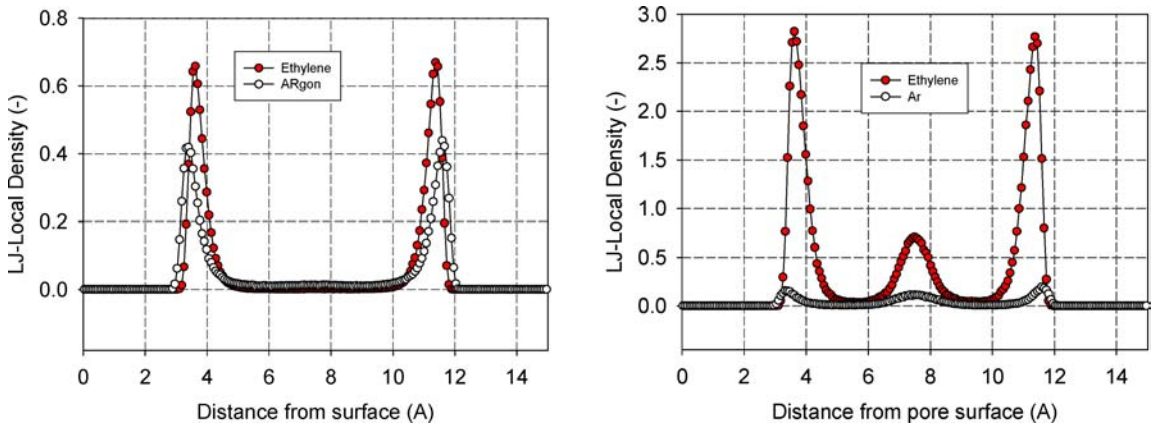

Figure 5. Local density distribution of ethylene and argon for (a) co-operative region and (b) competitive region.

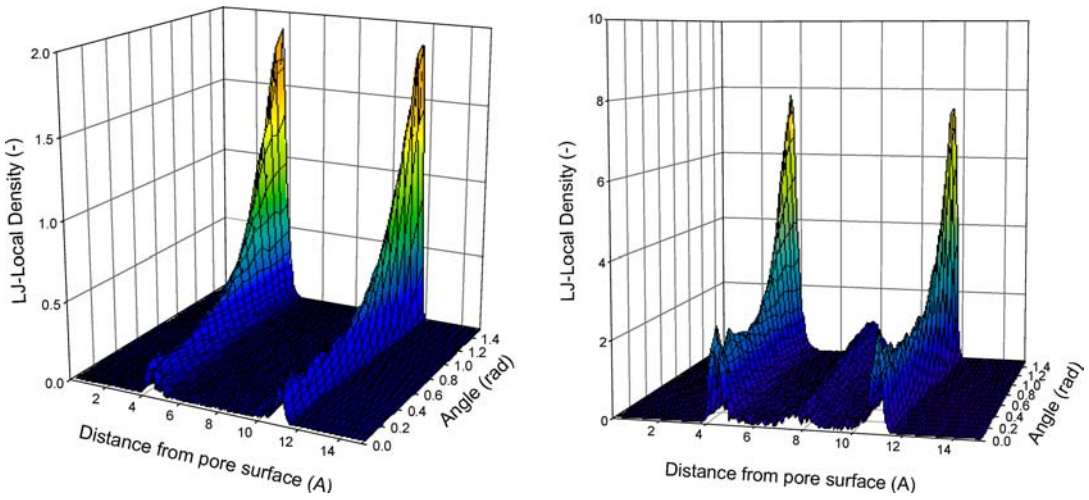

Figure 6. 3D-local density distribution of ethylene versus distance and angle θ (a) Ethylene partial pressure = 1,500 Pa (co-operative adsorption); (b) ethylene partial pressure = 10,000 Pa (competitive adsorption).

adsorption of ethylene compared to the case of pure ethylene. However, in the *competitive* region (partial pressure of ethylene is 10,000 Pa), the dominance of ethylene is clearly seen in all three layers inside the pore (Fig. 5(b)). This is due to the stronger affinity of ethylene with the surface. The three peaks of argon are much lower than those for ethylene, and we note that the peaks of argon are quite comparable in all layers despite the weaker solid-fluid interaction of argon and the super-critical nature of argon. This is attributed to the fluid-fluid interaction between argon and ethylene molecules in all three layers.

The orientation of ethylene molecule in these two regions is shown in Fig. 6 as plots of local density versus distance from the pore surface and the angle between ethylene molecular axis and the z-axis. The angle of zero means vertical orientation and $\pi/2$ means for parallel orientation. In the co-operative region (Fig. 6(a)), the orientation of ethylene is dominantly parallel to the surface. This parallel orientation persists in the competitive region for the two contact layers (Fig. 6(b)) although there is an increase in the population of molecules having a vertical orientation. This is simply due to the effect of fluid-fluid interaction between molecules in the contact layers and those in the inner core layer. On the other hand, ethylene molecules in the inner core have no preferential orientation, although parallel orientation is slightly preferred.

This is mainly due to the dominance of the fluid-fluid interaction.

3.2. *Ethylene-Nitrogen Mixture*

We now consider a system of ethylene/nitrogen mixture. The reason for investigating this is that nitrogen is quite commonly used as a carrier for chromatographic study and nitrogen carries discrete charges (in contrast to no charge on argon molecule). Let us consider this system for a 10 A slit pore. The calculations of the dispersive interaction were carried out with the minimum image convention, while those of electrostatic interaction were done directly among charges (including images) when the cut-off is less than a threshold value, beyond which we use the long range correction proposed by Heyes and van Swol (1980).

The conclusions about the cooperation and competition obtained earlier for argon are also observed for nitrogen, as shown in the following figure (Fig. 7) where we plot the ethylene amount adsorbed versus the ethylene partial pressure at 200 K with a 10 A slit pore. The nitrogen partial pressure is maintained constant at 1 atmosphere (1.013×10^5 Pa). As seen in this figure, at low pressures when the surface is under-saturated, the presence of carrier gas in fact helps to increase the amount of ethylene adsorbed. This is the cooperative effect as a result of the interaction between the ethylene molecules and nitrogen molecules on the surface, the same of conclusion observed earlier with argon. When pressure is increased beyond 120 Pa, the surface is now fairly loaded with molecules and this is when the competition between ethylene and nitrogen for the finite surface area available for adsorption occurs. As a result of this competition, the amount of ethylene adsorbed is less than that when ethylene is the only component in the gaseous phase.

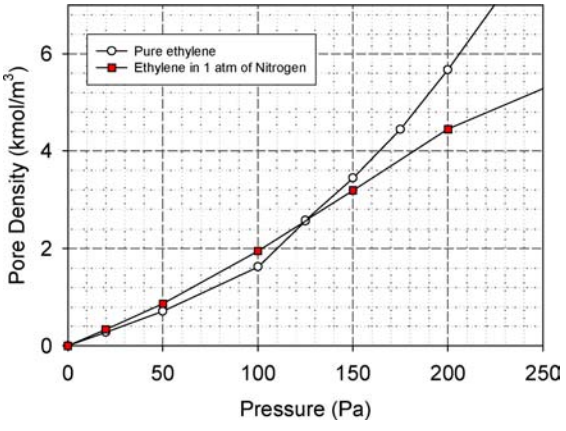

Figure 7. Adsorption isotherm of ethylene in slit pore of 10 A pore width (filled circle: mixture; empty circle: pure component).

3.3. *Ethylene-Ethane Adsorption*

Next we simulate the adsorption of ethylene and ethane at 200 K to illustrate further the cooperation and competition effects on the mixture adsorption. At this temperature, both ethylene and ethane are sub-critical fluids. Let us start with mixture adsorption in 10 A slit pore.

H = 10 A

Figure 8(a) shows the adsorption isotherm of ethylene, plotted as the pore density versus its partial pressure for the case of mixture, and for the case of pure component as pore density versus the ethylene pressure. In the case of mixture, the gaseous mole fraction of ethylene is 0.5. The curve with unfilled symbols is for the case of pure ethylene while that with filled symbols is for the case of mixture. For the low pressure range where the surface loading is less than that required to form a monolayer, the isotherm for the case of mixture is greater than that for the case of pure ethylene. This is the cooperative effect of interaction between adsorbed molecules of like species as well as that between unlike species that we have discussed earlier. When the pressure is increased, we observe the competition and the isotherms of ethylene and ethane in mixture is clearly less than the isotherms for pure component. Figure 8(b) shows the adsorption of stronger-adsorbing species (ethane) and we see that the effect of cooperative phenomenon is less with the strongly adsorbing component. This is because the presence of the weaker adsorbing species does not significantly increase the interaction among all adsorbed molecules.

H = 15 A

Like the case of ethylene/argon we have dealt with earlier in Fig. 4, we expect again here that the effect of cooperative is lesser in importance in the case of larger pores compared to smaller pores. Figure 9 shows the adsorption of mixture of ethylene and ethane in 15 A

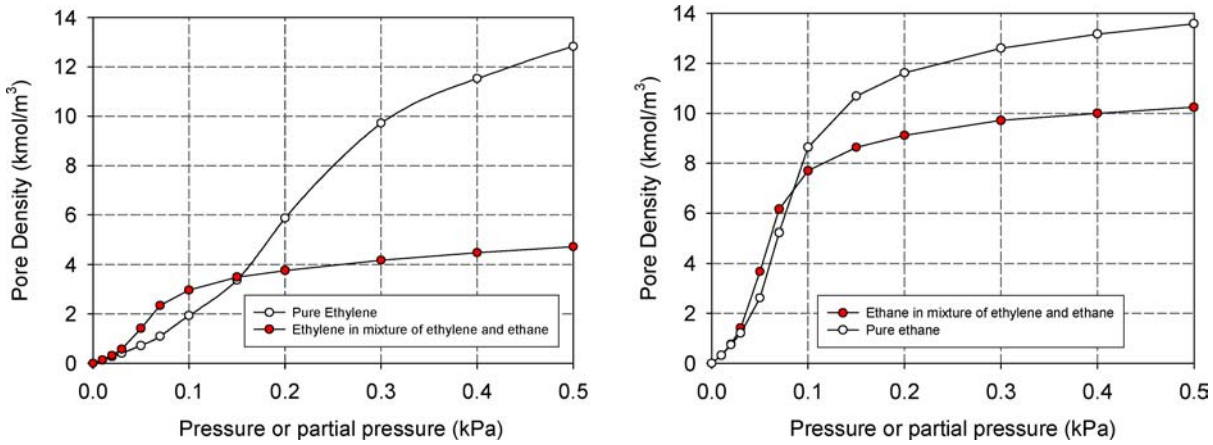

Figure 8. Adsorption isotherm of (a) ethylene and (b) ethane in slit pore of 10 A pore width.

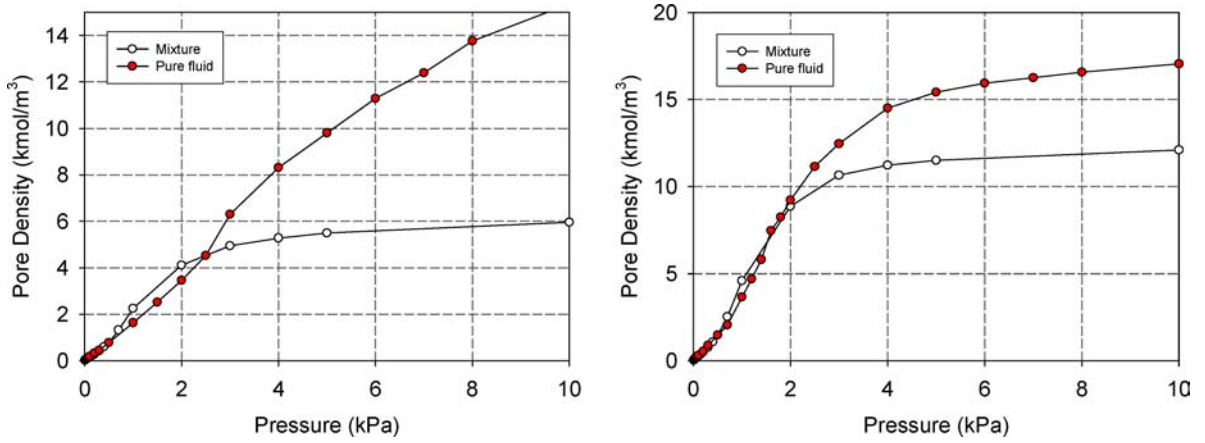

Figure 9. Adsorption isotherm of (a) ethylene and (b) ethane in slit pore of 10 A pore width.

slit pore. The mole fraction of ethylene in the gas phase is 0.5. The phenomena of *co-operation* and competition also observed here for 15 A, but the effect is less than that observed for 10 A.

The distribution of ethylene and ethane in the region of cooperation is shown in Fig. 10(a), while that in the region of competition is shown in Fig. 10(b). The pressure used in Fig. 10(a) is 1,000 Pa, at which the total number of molecule of ethylene and ethane is less than that required to form a complete monolayer. We have co-operative adsorption. On the other hand, the pressure used in Fig. 10(b) is 10,000 Pa, at which the two contact layers close to the two walls are completely covered with adsorbed molecules and the layer in the middle is also filled with adsorbed molecules. The spread of the middle peak is greater than that of the peaks of the contact layers. This is due to the weaker solid-fluid interaction of the inner core layer. We also note in Fig. 10 the dominance of ethane over ethylene in all layers.

To understand the orientation of ethylene and ethane in each layer, we plot in Fig. 11 the 3D-local density distribution of these species versus distance from the pore surface and the angle formed between the molecular axis and the z-coordinate. In the region of pressure in which we have cooperative adsorption, the two contact layers have concentrations less than the monolayer coverage and the orientation of ethylene and ethane in this region of cooperative adsorption adopt preferentially the parallel orientation (the angle is $\pi/2$). The

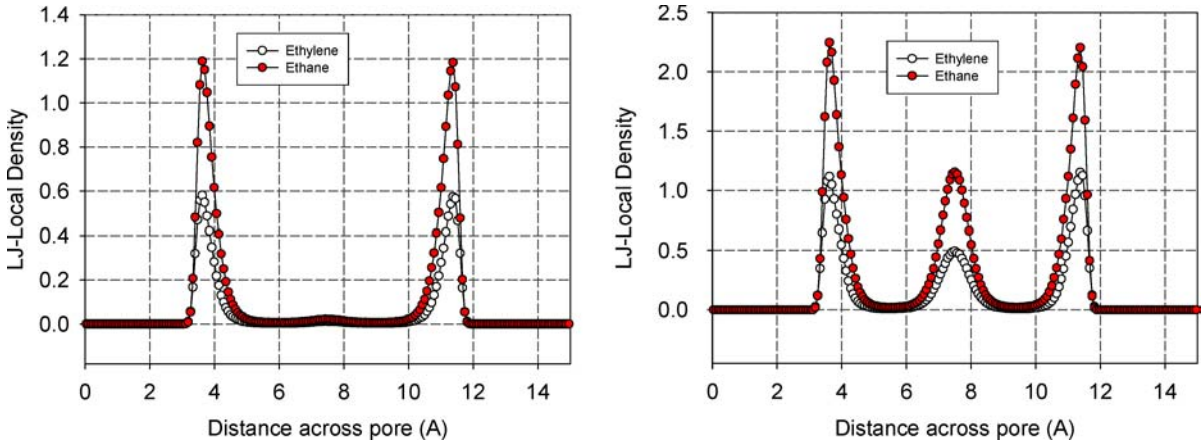

Figure 10. Local distribution of ethylene and ethane in the (a) co-operation region and (b) competitive region.

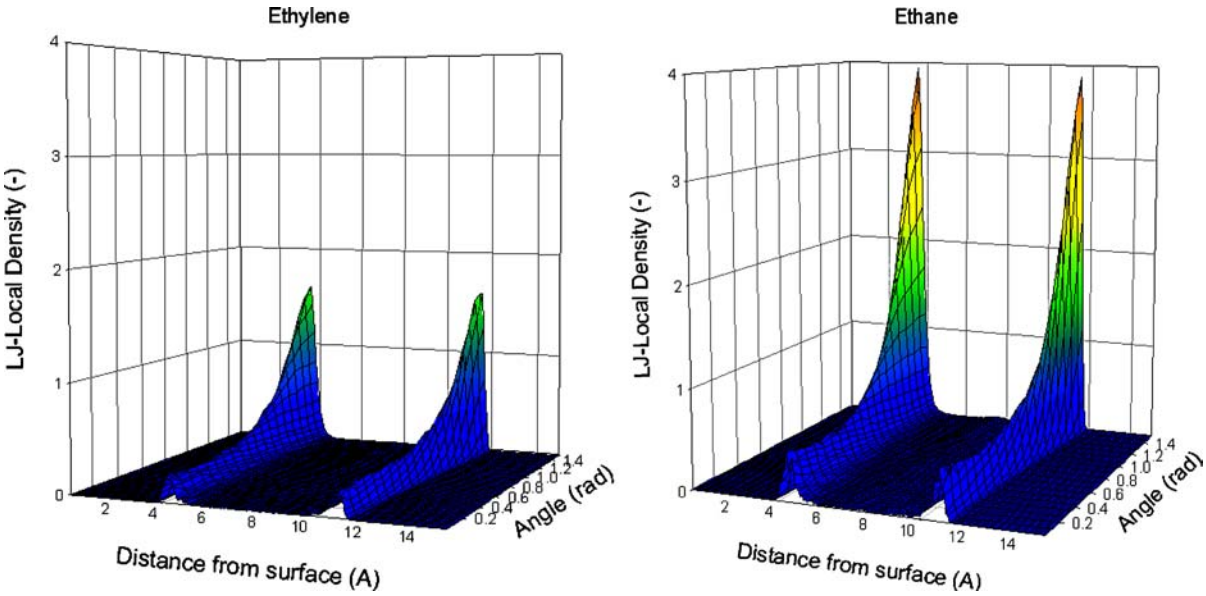

Figure 11. 3D-Local distribution of (a) ethylene and (b) ethane in the co-operation region.

higher peak of ethane in Fig. 11 supports the dominance of ethane over ethylene.

In the region of competitive adsorption, the three layers in this 15A pore are filled with ethylene and ethane molecules (Fig. 10(b)). The orientations of these two species are shown in Fig. 12. In the contact layers, ethylene and ethane both prefer parallel orientation with the surface, while in the inner core layer both species do not have any preferential orientation although ethane molecules have a slight dominant parallel orientation. The somewhat random orientation of ethylene and ethane in the inner core layer is due to the stronger influence of fluid-fluid interaction compared to the solid-fluid interaction, while the slight dominant parallel orientation of ethane in the inner core is due to its stronger solid-fluid interaction.

$H = 20\ A$

Let us now consider a larger pore 20 A. With this width there are four layers that can be accommodated in the

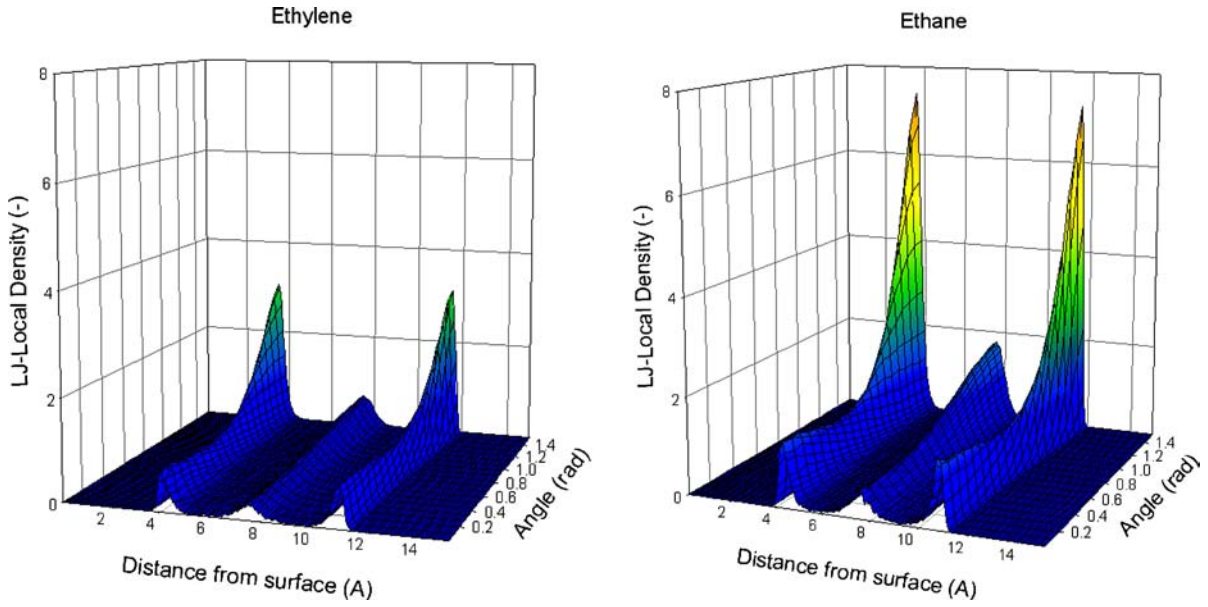

Figure 12. 3D-Local distribution of (a) ethylene and (b) ethane in the competitive region.

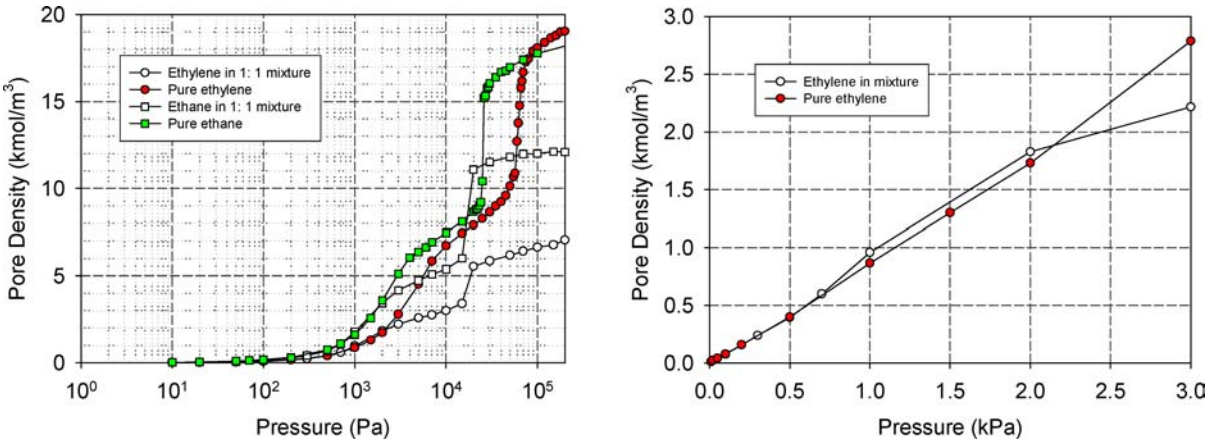

Figure 13. Adsorption isotherms of ethylene and ethane in 20 A pore (a) high pressure region (b) low pressure region.

pore. Figure 13 shows the adsorption isotherms of ethylene and ethane in the case of mixture (1:1 ratio of ethylene and ethane in the gas phase) as well as those for the case of pure components. For the case of mixture, the isotherms of ethylene and ethane are plotted versus their respective partial pressures.

For this pore, the pure component isotherms of ethane (filled square symbol) and ethylene (filled circle symbol) exhibit a 3D transition of pore filling. The 3D transition pressure of ethane is lower than that of ethylene, and this is due to its stronger affinity with the surface. In the case of mixture, the 3D transition pressure is between the pure component transition pressures. The 3D transition pressures of pure ethane and ethylene are 22,000 and 65,000 Pa, respectively, while the 3D transition pressure of mixture of ethylene and ethane (1:1) is about 36,000 Pa. Even with this large pore we still observe the cooperative adsorption (Fig. 13(b)), but this cooperation is very small compared to that observed in smaller pores.

The distribution of ethylene and ethane in the case of mixture is shown in Fig. 14 for two values of

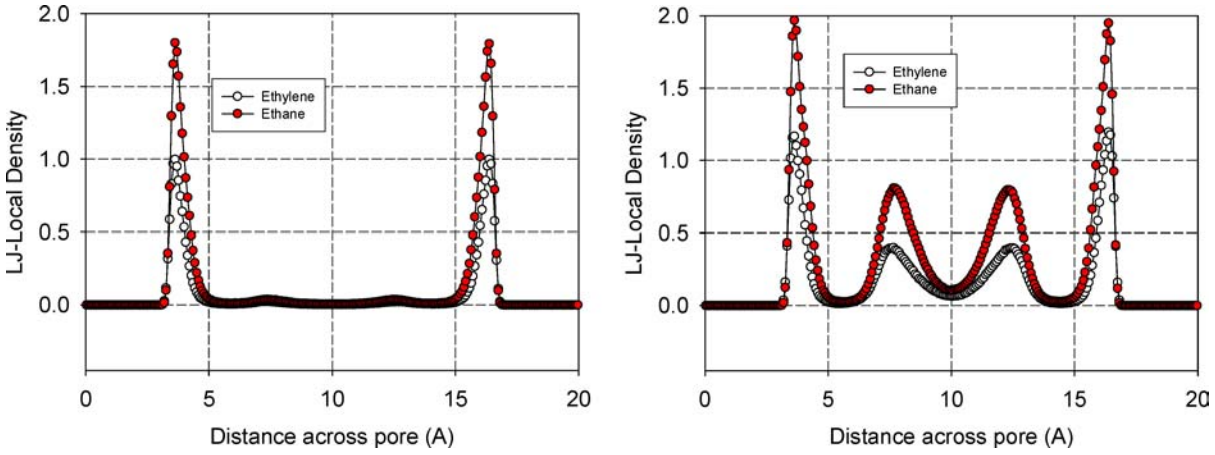

Figure 14. Local distribution of ethylene and ethane in the (a) co-operation region and (b) competitive region.

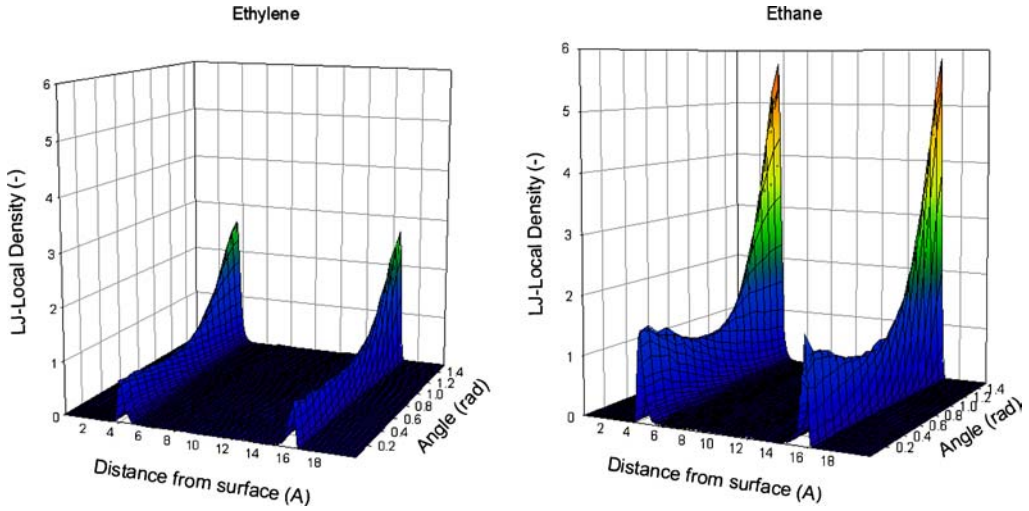

Figure 15. 3D-Local distribution of (a) ethylene and (b) ethane in the co-operative region for 20 A pore.

pressure. One is in the cooperative adsorption region while the other is in the competitive adsorption. The molecular layering is observed for all layers, and the dominance of ethane is also observed in all layers.

The orientation of ethylene and ethane is shown in Figs. 15 and 16 for $P = 10,000$ Pa and $P =$ 100,000 Pa, respectively. Like all previous cases the dominant orientation of the contact layers is the parallel orientation. However in the competitive adsorption region the vertical orientation of the contact layer is becoming significant although the parallel orientation is still dominant. This is due to the combined effects of fluid-fluid interaction between layers and the weaker solid-fluid interaction in larger pores. For the two inner core layers, there is no preference in the orientation.

Graphitized Thermal Carbon Black Surface

Now we consider the potential of the GCMC simulated results against the mixture data of ethylene and ethane on graphitized thermal carbon black at 298 K. The data are taken from Friederich (1970). At this temperature, we match the GCMC results against the pure component isotherms of ethylene and ethane to obtain the following values for the binary interaction parameters, $k = -0.027$ and -0.012, for ethylene and

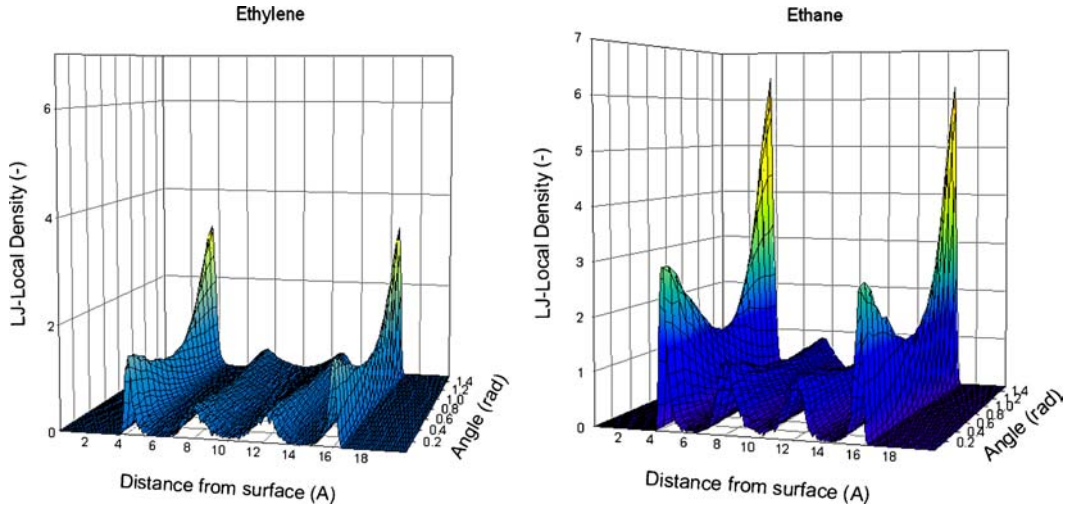

Figure 16. 3D-Local distribution of (a) ethylene and (b) ethane in the competitive region for 20 A pore.

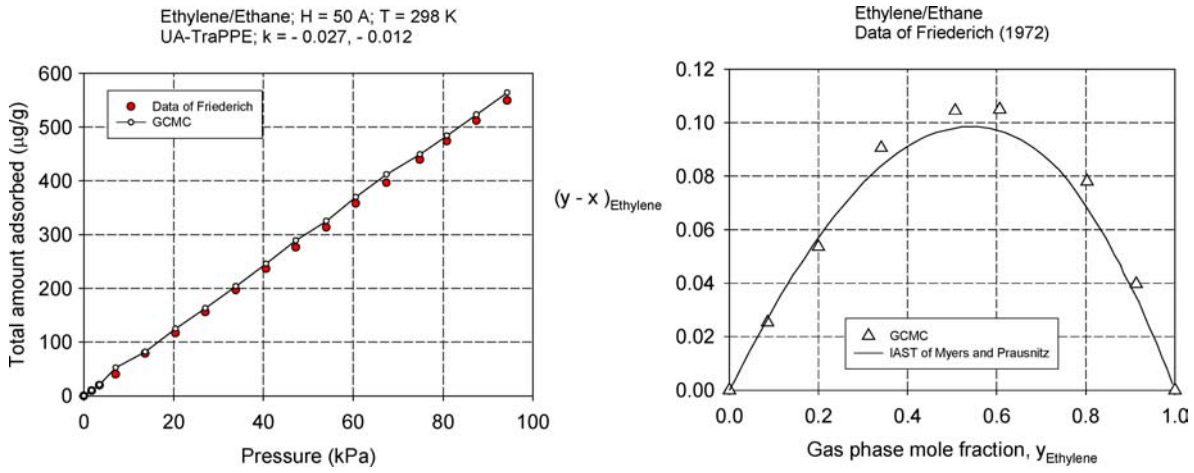

Figure 17. (a) Plot of the total amount adsorbed versus total pressure for ethylene/ethane adsorption on graphitized thermal carbon black; (b) plot of the (y-x) versus gas mole fraction of ethylene.

ethane, respectively. Having this information we simulate the mixture isotherms at various gas phase compositions used in the work of Friederich (mole fractions of ethylene are 0.086, 0.2, 0.341, 0.507, 0.607, 0.803 and 0.913). In all these cases the GCMC simulation results agree very well with the experimental results. We present below for the case of mole of fraction of ethylene of 0.507 in the form of a plot of the total amount adsorbed versus the total pressure (Fig. 17(a)) to show the agreement between the GCMC simulation results and the data. Figure 17(b) shows the plot of the difference of the gaseous mole fraction and the adsorbed phase mole fraction of ethylene versus the gaseous mole fraction of ethylene at a total pressure of 100,000 Pa. Also shown in this figure are the results calculated by the IAST theory. The agreement between the IAST and the GCMC simulation results is good, and that comes as no surprise as ethylene and ethane are comparable in molecule properties.

4. Conclusions

We have presented in this paper the potential of GCMC simulation as a useful tool to study adsorption microscopic behavior of linear molecules in slit pores and on

graphitized thermal carbon black. At pressures where the surface is only fractionally covered, we have co-operative adsorption irrespective of whether the fluid is sub- or super-critical. Orientation of molecules in the contact layer is dominantly parallel to the surface. At higher pressures where the contact layers are completely filled, we have competitive adsorption, and yet again the orientation of molecules in the contact layer is parallel although some vertical orientation is observed and it is due to the fluid-fluid interaction between layers, while that in second and higher layers shows no preferential orientation. We have shown in some details the co-operation and competition in adsorption of mixture with a number of systems involving ethylene, ethane, nitrogen and argon, and in pores of various sizes. The simulation results were tested against the experimental results of ethylene/ethane adsorption on graphitized thermal carbon black, and the agreement was found to be very satisfactorily.

Acknowledgment

This project is supported by the Australian Research Council.

References

Adams, D.J., "Grand Canonical Ensemble Monte Carlo for a LJ Fluid," *Mol. Phys*., **29**, 307–311 (1975).

Allen, M.P. and D.J. Tildesley, *Computer Simulation of Liquids*, Clarendon Press, Oxford, 1987.

Avgul, N.N. and A.V. Kiselev, "Physical Adsorption of Gases and Vapors on Graphitized Carbon Blacks," *Chemistry and Physics of Carbon*, **6**, 1–124 (1970).

Chen, B. and J. Siepmann, "Transferable Potentials for Phase Equilibria. 3. Explicit Hydrogen Description of Normal Alkanes," *J. Phys. Chem. B*., **103**, 5370–5379 (1999).

Costa, E., J.L. Sotelo, G. Calleja, and C. Marron, "Adsorption of Binary and Ternary Hydrocarbon Gas Mixtures on Activated Carbon: Experimental Determination and Theoretical Prediction of the Ternary Equilibrium Data," *AIChE J*., **27**, 5–12 (1981).

Costa, E., G. Calleja, C. Marron, A. Jimanez, and J. Pau, "Equilibrium Adsorption of Methane, Ethane, Ethylene, Propylene and Their Mixtures on Activated Carbon," *L. Chem. Eng. Data*, **34**, 156–160 (1989).

Cracknell, R., D. Nicholson, and N. Quirke, "A Grand Monte Carlo Study of Lennard-Jones Mixtures in Slit Shaped Pores," *Mol. Phys*., **80**, 885–897 (1993).

Do, D.D. and H.D. Do, "Adsorption of Ethylene on Graphitized Thermal Carbon Black and in Slit Pores: A Computer Simulation Study," *Langmuir*, **20**, 7106 (2004).

Friedrich, R.O., "Determination of Binary Adsorption Equilibria of Ethylene-Ethane, Ethane-Propane and Propylene-Propane on Highly Graphitized Carbon at 25 C and Pressures Below one atm," PhD thesis, Clemson University, 1970.

Friedrich, R.O. and J. Mullins, "Adsorption Equilibria of Binary Hydrocarbon Mixtures on Homogeneous Carbon Black at 25 C," *Ind. Eng. Chem. Fund*., **11**, 439–445 (1972).

Gardner, L., M. Kruk, and M. Jaroniec, "Reference Data for Argon Adsorption on Graphitized and Nongraphitized Carbon Blacks," *Journal of Physical Chemistry B*, **105**(50), 12516–12523 (2001).

Heyes, D.M. and F. van Swol, "The Electrostatic Potential and Field in the Surface Region of Lamina and Semi-Infinite Point Charge Lattice," *J. Chem. Phys*., **75**, 5051–5058 (1981).

Jaroniec, M. and R. Madey, *Physical Adsorption on Heterogeneous Solids*, Elsevier, Amsterdam, 1988.

Kaul, B., "Correlation and Prediction of Adsorption Isotherm Data for Pure and Mixed Gases," *Eng. Chem. Proc. Des. Dev*., **23**, 711–716 (1984).

Keller, J.U., F. Dreisbach, H. Rave, R. Staudt, and M. Tomola, "Measurement of Gas Mixture Adsorption Equilibria of Natural Gas Compounds on Microporous Sorbents," *Adsorption*, **5**, 199–214 (1999).

Kruk, M., Z. Li, M. Jaroniec, and W.R. Betz, "Nitrogen Adsorption Study of Surface Properties of Graphitized Carbon Blacks," *Langmuir*, **15**, 1435–1441 (1999).

Lastoskie, C., K.E. Gubbins, and N. Quirke, "Pore Size Heterogeneity and the Carbon Slit Pore: A Density Functional Theory Model," *Langmuir* **9**(10), 2693–2702 (1993a).

Lastoskie, C., K.E. Gubbins, and N. Quirke, "Pore Size Distribution Analysis of Microporous Carbons: A Density Functional Theory Approach," *Journal of Physical Chemistry*, **97**(18), 4786–4796 (1993b).

Lastoskie, C.M. N. Quirke, K.E. Gubbins, "Structure of Porous Adsorbents: Analysis Using Density Functional Theory and Molecular Simulation," Studies in Surface Science and Catalysis, *Equilibria and Dynamics of Gas Adsorption on Heterogeneous Solid Surfaces*, **104**, 745–775 (1997).

LeVan, M.D. and T. Vermeulen, "Binary Langmuir and Freundlich Isotherms for Ideal Adsorbed Solutions," *J. Phys. Chem*., **85**, 3247–3250 (1981).

Martin, M. and J. Siepmann, "Transferable Potentials for Phase Equilibria. 1. United Atom Description of Normal Alkanes," *J. Phys. Chem. B*., **102**, 2569–2577 (1998).

Moon, H. and C. Tien, "Further Work on Multicomponent Adsorption Equilibria Calculations Based on the Ideal Adsorbed Solution Theory," *Ind. Eng. Chem. Res*., **26**, 2042–2047 (1987).

Murthy, C.S., S.F. O-Shea, and I.R. McDonald, "Electrostatic Interactions in Molecular Crystals. Lattice Dynamics of Solid Nitrogen and Carbon Dioxide," *Mol. Phys*., **50**, 531–541 (1983).

Myers, A.L. and J.M. Prausnitz, "Thermodynamics of Mixed Gas Adsorption," *AIChE J*., **11**, 121–127 (1965).

Nicholson, D. and N.G. Parsonage, *Computer Simulation and the Statistical Mechanics of Adsorption*, Academic Press, London, 1982.

Norman, G.E. and Filinov, "Investigation of Phase Transitions by a Monte Carlo Method," *High Temperature* (*USSR*), **7**, 216–222 (1969).

Olivier, J.P. "Modeling Physical Adsorption on Porous and Nonporous Solids Using Density Functional Theory," *Journal of Porous Materials*, **2**(1), 9–17 (1995).

Reich, R., W. Ziegler, and K. Rogers, "Adsorption of Methane, Ethane, and Ethylene Gases and Their Binary and Ternary

Mixtures and Carbon Dioxide on Activated Carbon at 212–301 K and Pressures to 35 atm.," *Ind. Eng. Chem. Proc. Des. Dev*., **19**, 336–344 (1980).

Russell, B. and M.D. LeVan, "Group Contribution Theory for Adsorption of Gas Mixtures on Solid Surfaces," *Chem. Eng. Sci*., **51**, 4025–4038 (1996).

Russell, B. and M.D. LeVan, "Co-adsorption of Organic Compounds and Water Vapor on BPL Activated Carbon. 3. Ethane, Propane and Mixing Rules," *Ind. Eng. Chem. Res*., **36**, 2380–2389 (1997).

Staudt, R., F. Dreisbach, and J.U. Keller, "Correlation and Calculation of Multicomponent Adsorption Equilibria Data Using a Generalized Adsorption Isotherm," *Adsorption*, **4**, 57–62 (1998).

Steele, W.A., "Physical Interaction of Gases with Crystalline Solids. I. Gas-Solid Energies and Properties of Isolated Adsorbed Atoms," *Surface Science*, **36**(1), 317–352 (1973).

Steele, W.A., "International Encyclopedia of Physical Chemistry and Chemical Physics, Topic 14, Vol. 3: The Interaction of Gases with Solid Surfaces" (1974).

Steele, W.A. "Computer Simulations of the Structural and Thermodynamic Properties of Adsorbed Phases," *Surfactant Science Series*, *Surfaces of Nanoparticles and Porous Materials*, **78**, 319–354 (1999).

Steele, W.A. "Computer Simulations of Physical Adsorption: A Historical Review," *Appl. Surf. Sci.* **196**(1–4), 3–12 (2002).

Taqvi, S.M. and M.D. LeVan, "Virial Description of Two-Component Adsorption on Homogeneous and Heterogeneous Surfaces," *Ind. Eng. Chem. Res*., **36**, 2197–2206 (1997).

P.A. Tipler, *Physics*, Freeman and Company/Worth Publishers, New York, 1999.

Valenzuela, D.P. and A.L. Myers, *Adsorption Equilibrium Data Handbook*, Prentice Hall, New Jersey, 1989.

Wick, C.D., M. Martin, and J. Siepmann, "Transferable Potentials for Phase Equilibria. 4. United-Atom Description of Linear and Branched Alkenes and Alkylbenzenes," *J. Phys. Chem. B*., **104**, 8008–8016 (2000).

Yang, R.T., *Gas Separation by Adsorption Processes*, Butterworths, Boston, 1987.